Science in China: *Series D Earth Sciences* 2006 Vol.49 No.7 755—763

DOI: 10.1007/s11430-006-0755-0

Monitoring of rice crop using ENVISAT ASAR data

DONG Yanfang[1, 2], SUN Guoqing[1,3] & PANG Yong[4]

1. State Key Laboratory of Remote Sensing Science, Institute of Remote Sensing Applications, Chinese Academy of Sciences, Beijing 100101, China;
2. Graduate University of Chinese Academy of Sciences, Beijing 100039, China;
3. Department of Geography, University of Maryland, College Park, MD 20742, USA;
4. Forest Remote Sensing Lab, Research Institute of Forest Resource and Information Technology, Chinese Academy of Forestry, Beijing 100091, China

Correspondence should be addressed to Dong Yanfang (email: yfdong314@yahoo.com.cn)

Received October 8, 2004; accepted April 8, 2005

Abstract Because of the cloudy conditions during the rice growth period, rice is one of the agricultural crops most suited to monitoring with the SAR instruments. Backscatter response measured by SAR is correlated with rice conditions, including height, density, biomass and structure, which are variable at different growing stages. In this paper, multi-date ENVISAT ASAR Alternating Polarization Mode (APMode) imageries were acquired during the rice crop growing cycle. At the same time, the rice parameters were measured in field. A continuous canopy model was used to compute the backscattering from rice fields during the growth cycle, and the relationship between rice parameters and radar backscattering coefficients from both ASAR and modeling was analyzed. The effects of polarization, incidence angle and polarization on radar backscattering coefficients were analyzed. It was found that simulated radar backscatter has similar trends as ASAR data. This will be meaningful for the further research of rice parameters estimation from ASAR data. Different features show significantly different signatures in ASAR images and they follow some certain laws, so rice area can be accurately mapped by using multi-temporal SAR images, then rice yield can be estimated.

Keywords: rice, ASAR, radar backscattering, model.

Rice is the most important food source for people and is cultivated in most countries, among which China is one of the most productive. Increase of the world population and demands for economic development lead to the need of an efficient monitoring system for rice cultivation and forecasting of rice yield. Conventional methods for rice monitoring are based on ground-collected statistics, which is time consuming, inaccurate and expensive. Since the 1980s, satellite remote sensing has been considered as an important component in most crop monitoring programs. However, optical satellite data are hampered by poor weather conditions. Thus, the all-weather radar satellite offers an effective alternative to these traditional methods for the monitoring of rice crop[1,2].

Synthetic Aperture Radar (SAR) is all-day, all-weather instrument. It transmits radar signals and then measures how strongly those signals are scattered back. Radar's longer wavelengths make radar waves relatively undistorted by clouds. Because of the cloudy conditions during the rice growth period, rice is one of the agricultural crops most suitable to be monitored

with SAR instruments.

In different growing stages, crop has different conditions (height, structure, moisture content, and so on). All these factors affect the radar return signal[3 − 5]. Otherwise for different crop types, there are different correlations between crop parameters and radar backscatter signatures, studies have shown that rice backscattering coefficients are functions of plant height and biomass[6], through these functions rice parameters can be estimated. In addition, radar parameters such as wavelength, incidence angle and polarization also affect the received backscattering from targets. A vegetation canopy will interact with radar waves as a group of volume scatters. In general, shorter wavelengths, of approximately 2 to 6 cm, are best for sensing crop canopies and tree leaves, because at these wavelengths volume scattering is predominant and surface scattering from the underlying soil is minimized. Another factor influencing the effect of radar backscatter from vegetation is the polarization of the beam, with like-polarized waves (HH or VV) penetrating vegetation more than cross-polarized (HV or VH) waves.

In 1989, Le Toan *et al*.[7] used a theoretical model to interpret rice field measurements, in which rice canopy was taken as a collection of dielectric cylinders above water surface. Shao Yun *et al*.[8] used a calibration equation for RADARSAT to convert the DN of the image to backscatter coefficients (dB), then analyzed the relationship between rice growing stage and backscatter coefficients. And in 2002, Shao Yun *et al*.[9] compared the simulations from a empirical model with SAR image measurements. Le Toan *et al*.[2] developed a method using theoretical modeling to interpret observations from ERS-1 and ERS-2 data. The backscattering is calculated by Monte Carlo simulations of scattering from dielectric cylinders and elliptical discs over a dielectric half space using the Foldy-Lax multiple scattering equations. Inoue *et al*.[10] investigated the relationships between microwave backscatter signatures and rice canopy growth variables using multi-frequency and full-polarization data, and fitted the scatter from the rice into an empirical equation. Zeng Qiming *et al*.[11] constructed several sub-models for rice backscattering based on the Vector Radiative Transfer (VTR) theory, then an integrated model for the first-order scattering mechanisms is achieved for simulating rice backscattering coefficient.

The new generation of ASAR instrument (launched on March 1, 2002) on-board ENVISAT works at C-band (wavelength 5.6 cm), for which the canopy volume scattering dominates. Alternating Polarization Mode (APMode) product contains two co-registered images. In this paper, we used the AP product containing HH and HV polarization. In order to increase the temporal coverage, ASAR data from various beams of narrow swath were acquired. The effect of incidence angle on radar backscatter needs to be understood before the parameters retrieval algorithm could be developed. The modified model based on a continuous canopy model[12] was used for the purpose. Using field rice measurements as inputs radar backscattering at the same incidence angles as ASAR data were simulated. Comparisons of the model results with radar signatures indicated good agreements in polarization and angular trends.

1 Study area and rice growing conditions

The study area is flat and located in Northeast China's Jilin Province. Rice is one of the mainly agricultural crops in this area. Five different types of rice fields were selected, and the locations were marked with DGPS.

Due to the relatively cold weather conditions in Northeast China, there is only one rice season − from May to September. After sowing and transplanting, the field should be covered by water. About 2 weeks later, the important tillering phase starts and lasts for about one month. In this phase the plants build additional stems. Next is the reproductive phase, lasting another month. Here the panicles are formed and the plants flower. Vertical growth stops and the leaves become more horizontal. Finally the ripening phase takes another month. The moisture content of the plants decreases and they change color from full green to yellowish green. The supply of water is stopped about two weeks before harvest to dry the land.

During the rice growth cycle, rice parameters were measured for about 14 times. From sowing to heading, the stems are quasivertical and the leaves have a small insertion angle.

Plant height and plant biomass are analyzed as a

function of the plant growing stage (Figs. 1 and 2). In Fig. 1, the general increasing trend is observed for the rice height until the end of the productive stage, then remains stable and a slight decrease in the end because of the bend of head. In Fig. 2, the function is an exponent curve.

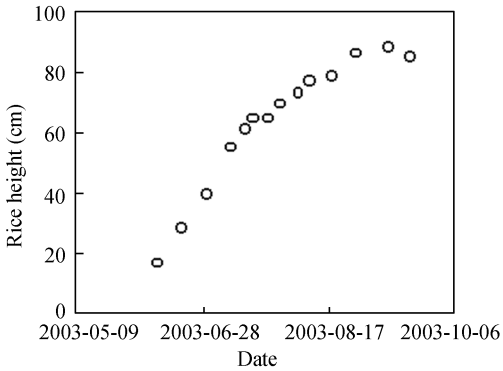

Fig. 1. Rice height as function of date.

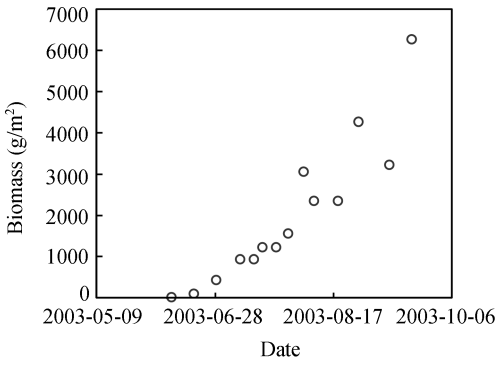

Fig. 2. Rice biomass as function of date.

With the appearance of spike, the rice plant's biomass increases more quickly. The data dispersion in the above 2 figures can be explained by different causes including sampling procedure, the within-field variability, and so on.

The water content of rice plant was 0.90 g/g during the first month after the transplanting stage. Then the water content dropped, but always kept in the range of 0.8—0.7 g/g. Just before the harvest season (late September), the water content dropped to 0.5—0.6 g/g.

2 ASAR data processing

An ENVISAT ASAR time-series was acquired in order to monitor a complete rice growing cycle. The nine ASAR data sets covered the period from 12 June to 11 October. The data sets included both descending and ascending passes, variable incidence angles and alternating polarization mode (HH and HV). An overview of all acquisitions is given in Table 1.

Table 1 ASAR data overview

Acquisition date	Incidence angle (°)
2003-06-12	37.5188255
2003-06-19	28.547904
2003-06-28	33.5688285
2003-07-14	28.544497
2003-07-24	28.565056
2003-08-02	33.58113
2003-08-05	40.9018435
2003-09-25	37.5176735
2003-10-11	33.577111

The ENVISAT ASAR instrument provides data with pixel sizes of 12.5 m and spatial resolution of 30 m. The backscattering coefficient σ^0 corresponding to the test fields was extracted from the images.

The relationship between the image intensity and the backscattering coefficient σ^0 is given by

$$\sigma^0 = \frac{\langle A^2 \rangle}{K} \sin(\alpha_d), \tag{1}$$

where σ^0 is the radar backscattering coefficient of distributed target to be measured; A is the image digital number; α_d is incidence angle at target position; K is absolute calibration factor for this product. Both K and α_d can be found in image header.

The AP Mode data are processed as follows:

(1) Data extraction (BEST used): header analysis, full resolution extraction, amplitude to power, backscattering image generation.

(2) Map projection converting: the user defined projection-NE China LCC projection was used.

(3) Co-registration: Subset all ASAR images to the same size, which covers the same area, then save 9 multi-temporal subset images to one ENVI standard file respectively for HH and HV polarization, in which each band represents one date. Thus two time-series ASAR data sets, HH and HV, were generated. Finally register the ENVI images to used coordinate system according to Ground Control Points (GCPs).

(4) The rice sample fields were figured out from ASAR images according to field GPS measurements.

(5) The mean backscatter coefficient values for each sample field were computed.

Ground data collected for each rice field on ASAR acquisition day included temperature, plant height, stem number, stem diameter, wet weight, dry weight, relative moisture content, leaf width, leaf length, leaf thickness, and water depth.

3 Model simulation and method

3.1 Model description

In the last few decades, several models widely used in vegetation microwave remote sensing researches are based on the radiative transfer theory with vegetation elements described as discrete dielectric scatters[13−17]. The model used in this study is a modified version of the continuous canopy model by Sun *et al*.[18]. The plant shape and size are considered as the model's inputs to simulate rice backscattering coefficient. The rice canopy is defined as the layer from above water to the top of the rice, including the stems (or branches) and leaves. The water is treated as specular surface, so the direct surface backscattering can be ignored in this simulation model. For the rice plants, four backscattering mechanisms are used in this model as depicted in Fig. 3. In eq. (2), the first term denotes the canopy volume scattering (Fig. 3(a)); the second term denotes canopy-water multiple scattering, resulting from the interaction between canopy and water surface (Fig. 3(b), (c) and (d)).

$$\sigma^0 = \sigma_v^0 + \sigma_{vw}^0. \quad (2)$$

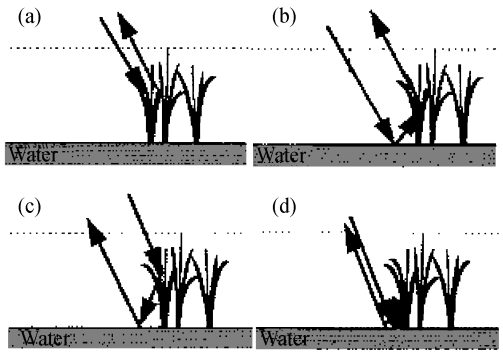

Fig. 3. Backscattering mechanisms in the rice canopy model. (a) Canopy volume scattering; (b) water-canopy; (c) canopy-water; (d) water-canopy-water).

3.2 Simulation method

We consider rice plants planted with nearly constant spacing over the sampled square area A (1 m^2), where there is N_b bunches. Each rice plant contains a bunch of N_s vertical preferred dielectric cylindrical stems with height h, radius a, and dielectric constant ε_s. Each rice stem has N_l leaves of rectangle shape with width w and length l, thickness d, and complex dielectric constant ε_l. The underlying water has a complex dielectric constant ε_1. We assume that the leaf orientation angle is uniformly distributed from zero to a maximum angle β, and the leaf azimuth angle and the stem azimuth angle are uniformly distributed from zero to 2π.

For stems, the scattering was calculated using the finite cylinder approximation. The returns from leaves were calculated using the physical optics approximation for rectangles. Model parameters are as follows:

(1) The plant height, plant gravimetric moisture content, leaf width, and leaf length are the mean values of field measurements.

(2) The stem radius, number of stem per m^3, number of bunches per m^3, number of leaves per stem, and leaf thickness are derived from measurements.

(3) Leaf tilt angles from stem to leaf are averaged from measurements.

(4) The dielectric constant of the underlying water is taken as ε_1= (80, 0).

(5) The canopy depth equals the plant height above water.

In this model, the dielectric constants for leaves and branches were calculated by Debye-Cole dual-dispersion model[19], which described the relationship between plant's water content (including bulk water and bound water) and complex dielectric constant. The water contents of rice leaves and stems were calculated from wet weight and dry weight.

The rice backscattering is mainly affected by the contribution of leaves and stems, so before the rice backscattering model is developed they should be modeled respectively at first.

Rice leaves were taken as rectangle discs, the transform from leaf coordinate system to local coordinate system was also done in the model. The geometrical parameters of one single leaf include length, width and the angle between the leaf's orientation to the stem's orientation. Assuming the rice stem is vertical, the angle was defined as leaf's azimuth angle.

The scattering matrix of a single rice leaf can be

described as eq. (3):

$$\begin{bmatrix} S_{vv} & S_{vh} \\ S_{hv} & S_{hh} \end{bmatrix}. \tag{3}$$

The attenuation matrix of a single rice leaf can be computed similarly as scattering matrix, taking the leaf size and orientation angle as averages of measurements, assuming the leaf's azimuth angles were uniformly distributed between $0-2\pi$. The single leaf's Stokes matrix can be computed from its scattering matrix. Eq. (4) is the 4×4 Stokes matrix,

$$\begin{bmatrix} |S_{vv}|^2 & |S_{vh}|^2 & \mathrm{Re}(S_{vh}{}^{*}S_{vv}) & -\mathrm{Im}(S_{vh}{}^{*}S_{vv}) \\ |S_{hv}|^2 & |S_{hh}|^2 & \mathrm{Re}(S_{hh}{}^{*}S_{hv}) & -\mathrm{Im}(S_{hh}{}^{*}S_{hv}) \\ 2\mathrm{Re}(S_{vv}{}^{*}S_{hv}) & 2\mathrm{Re}(S_{vh}S_{hh}{}^{*}) & S_{33} & S_{34} \\ 2\mathrm{Im}(S_{vv}{}^{*}S_{hv}) & 2\mathrm{Im}(S_{vh}S_{hh}{}^{*}) & S_{43} & S_{43} \end{bmatrix}, \tag{4}$$

where

$$S_{33} = \mathrm{Re}\ (S_{vv}S_{hh}{}^{*} + S_{vh}S_{hv}{}^{*}),$$

$$S_{34} = \mathrm{Im}\ (S_{vv}S_{hh}{}^{*} - S_{vh}S_{hv}{}^{*}),$$

$$S_{43} = \mathrm{Im}\ (S_{vv}S_{hh}{}^{*} + S_{vh}S_{hv}{}^{*}),$$

$$S_{44} = \mathrm{Re}\ (S_{vv}S_{hh}{}^{*} - S_{vh}S_{hv}{}^{*}).$$

The average scattering matrix and Stokes matrix of branches were calculated using Gaussian Quadratures integration, where branches were looked as homogeneous cylinders. The geometrical parameters of rice stems include stem height and stem diameter. The computation method is the same as leaf's.

The rice backscattering model presented in this paper is based on the first-order solution of Radiative Transfer Equation, which comprises 4 scattering mechanisms. At first, the scattering matrix and Stokes matrix of single leaf and single branch were computed respectively by using the method described above. Assuming the rice leaves and stems are uniformly distributed in the defined canopy space, multiplied by the number of leafs and branches per m^3 respectively, the sum of these two components becomes the rice canopy's volumetric scattering matrix and Stokes matrices. The forward scattering matrix was used to calculate the extinction of canopy. With the same method, the scattering matrix and Stokes matrix under other scattering mechanisms will be achieved. The sum of all is the total effects of rice canopy, demoted as $T_t(\theta_0)$. The whole rice canopy's backscattering coefficients for all polarizations can be computed from $T_t(\theta_0)$ as eq. (5), then σ^0 in eq. (2) can be achieved.

$$\sigma_{vv}^0 = 4\pi\cos(\theta_0)[T_t(\theta_0)]_{11}, \tag{5a}$$

$$\sigma_{hh}^0 = 4\pi\cos(\theta_0)[T_t(\theta_0)]_{22}, \tag{5b}$$

$$\sigma_{hv}^0 = 4\pi\cos(\theta_0)[T_t(\theta_0)]_{21}, \tag{5c}$$

$$\sigma_{vh}^0 = 4\pi\cos(\theta_0)[T_t(\theta_0)]_{12}. \tag{5d}$$

4 Results

In this part, we plot the relationship between the simulated results and field measurements. The backscattering coefficients were simulated for the five sample fields based on extensive ground truth measurements as model inputs. But for briefness, the study was only focused on one rice sample field, where the model inputs and ASAR measurements were from the corresponding rice field.

4.1 Relationship between simulated results and rice parameters

Fig. 4 shows the relationship between simulated backscattering coefficients and rice growth stage at incidence angels 28.5 degree. There is an increasing trend for both like-polarization (HH) and cross-polarization (HV). For HH polarization, the backscattering value is higher than HV polarization. The slight decrease at the end can be explained as the dying of rice plant before harvest.

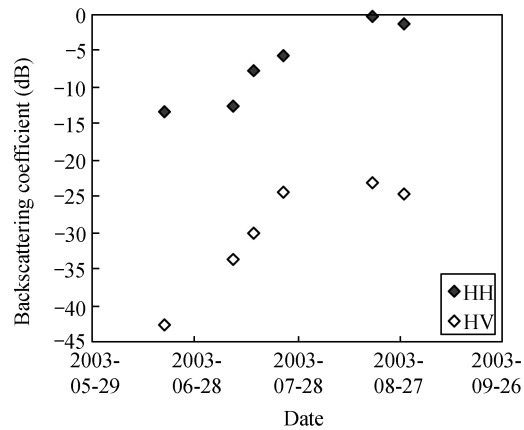

Fig. 4. Simulated backscattering coefficient versus date.

Simulated backscattering coefficient is strongly correlated with crop biomass and height (Figs. 5 and 6). They show that C-HV backscattering coefficients

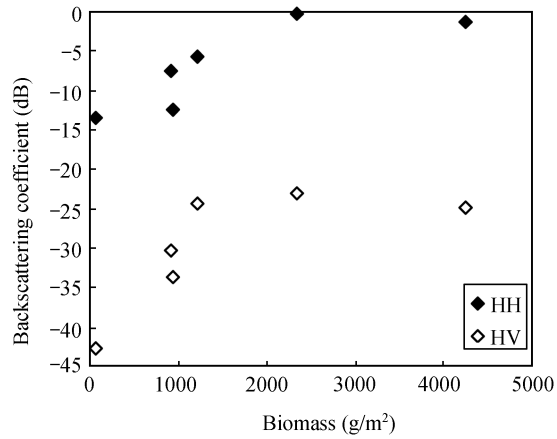

Fig. 5. Simulated backscattering coefficient versus rice biomass.

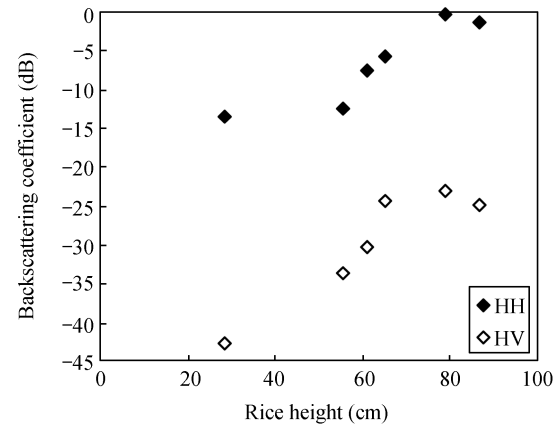

Fig. 6. Simulated backscattering coefficient versus rice height.

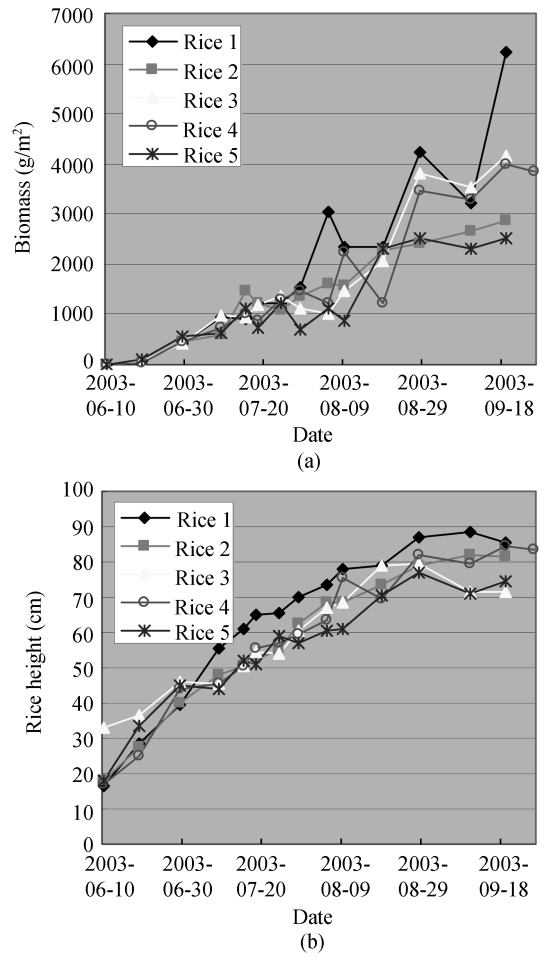

Fig. 7. Rice bio-parameters of five different rice fields. (a) Rice biomass; (b) rice height.

are better correlated with crop biomass and height than C-HH. In Figs. 5 and 6, the incidence angles both are 28.5°. The backscattering coefficients at incidence angles of 37.5° and 40.9° were also simulated. They also showed the similar trends with rice age, biomass and height. The HH polarization and smaller incidence angle were less well correlated with the biomass, while the cross-polarization was highly correlated.

4.2 Comparisons of five different rice fields

Five different rice fields have been selected for this research, and the same work has been done for each field. The results showed that ASAR and modeling backscattering coefficients had the similar simulation trends for the five fields, which have been presented in section 5. Fig. 7 shows the differences of bio-parameters of the 5 rice fields. For Rice 1, the biomass and height both are the highest among the five, so the backscattering coefficients are significantly higher than the other's. Fig. 8 shows the signatures on ASAR images for 5 different rice fields. Different backscattering coefficients can be seen for different rice conditions.

4.3 Rice area mapping

TM images have been widely applied to crop researches, but optical remote sensing is always impacted by bad weather. The all-weather microwave remote sensing makes sure that SAR images were dominantly advantageous for crop monitoring. In the composite images of Landsat TM band 2 (in red), band 5 (in green), and band 7 (in blue), the flooded rice fields and water area both show in red. But in SAR images they have very different intensity, so there show different backscattering coefficients, and these two features can be easily distinguished in

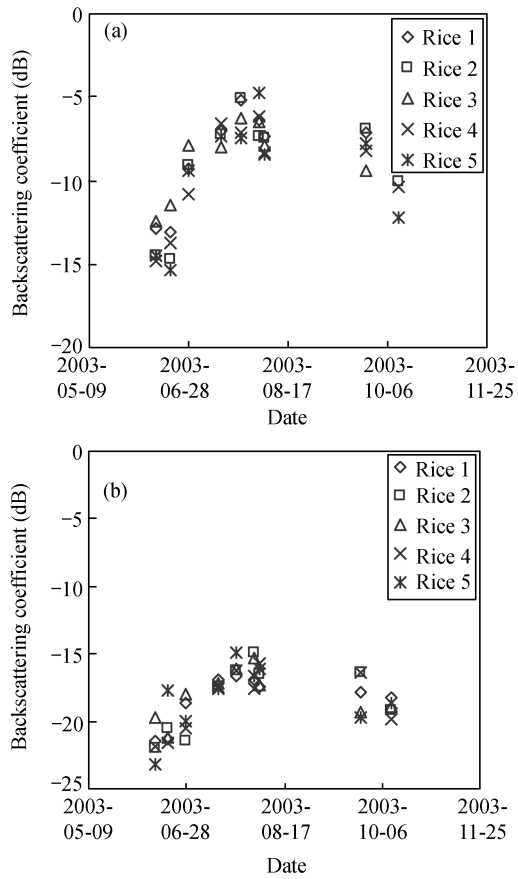

Fig. 8. ASAR measurements for five different rice fields. (a) HH polarization; (b) HV polarization.

ASAR images. Fig. 9(a) presents a composite of one TM image's band 2 (in red), band 5 (in green), and band 7 (in blue), in which red part in the center is rice field and the up-right cyan part is water. Fig. 9(b) presents the classification result of a composite of three-temporal ASAR images (HH polarization), June 19, 2003 (in red), July 14, 2003 (in green), August 5, 2003 (in blue). The parallel supervised classification method was used. Red denotes rice, up-right cyan denotes water, green denotes corn and blue denotes building. Seen from the results, rice area can be mapped from ASAR images. If the rice growing conditions can also be known, then rice yield can be estimated accurately.

The radar backscattering coefficients of rice, corn, water and building are shown in Fig. 10. Water has the lowest backscattering coefficient, and building has the highest. At the early stage of rice growth cycle, the backscattering coefficient of rice is about equal to that

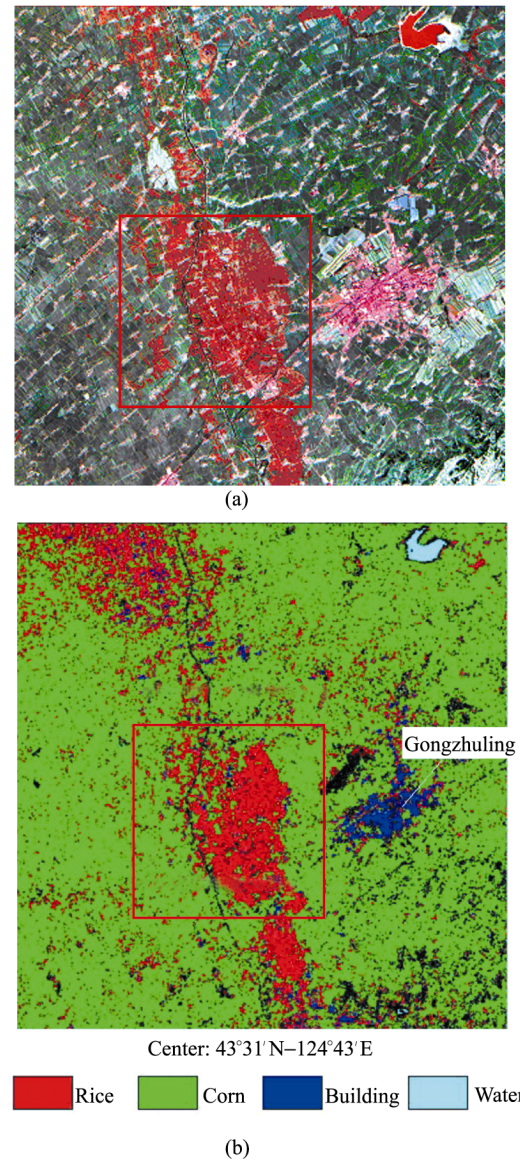

Fig. 9. TM image and classifications using ASAR images. (a) Composite of one TM image's band 2 (in red), band 5 (in green), and band 7 (in blue); (b) the classification result of a composite of three-temporal ASAR images.

of water, but then increases, saturates at the mature stage, and decreases at the harvest stage. Compared with rice, at the early stage corn has higher backscattering coefficient than rice, because there is rougher surface for corn field, while rice is covered by water. With the rice growing denser, the backscattering coefficient of rice is higher than that of corn.

5 Conclusions

In this paper, a radar backscattering model for rice

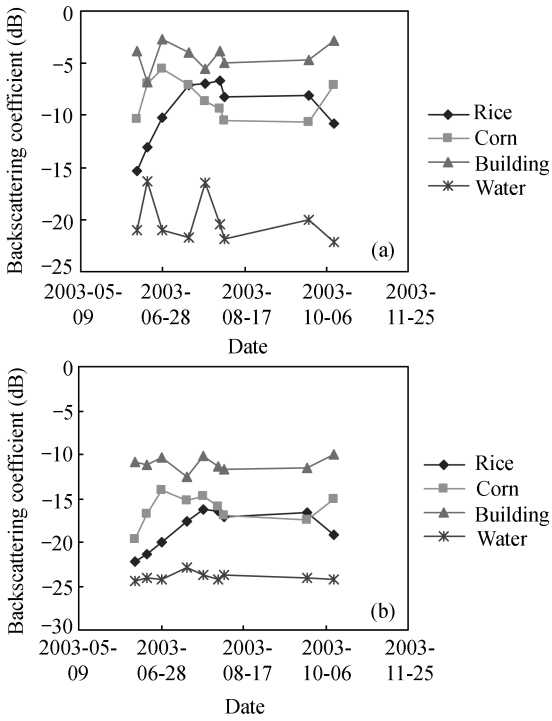

Fig. 10. Backscattering coefficients of four different features. (a) HH polarization; (b) HV polarization.

was developed through modifying the existing forest radar model. The field-measured rice parameters were used to simulate rice backscattering effects, and the results have been interpreted reasonably, simultaneously the temporal variation of rice backscattering was analyzed by using multi-date ASAR data. The correlation between ASAR data and rice parameters can be drawn both from ASAR images and model simulation results.

(1) Seen from the study of these five rice fields, σ^0, as the function of rice parameters (biomass, height), increases with the parameters, and saturate till the reproductive stage. For HH polarization, at the early stage, rice field had low backscattering coefficients (about −20 dB), but increased from −8 to −6 dB at the reproductive stage.

(2) It can be deduced from conclusion (1) that because in different growing stages rice has certain bio-parameters and shows different backscattering coefficients in SAR images, SAR data can be used to distinguish the rice growing stage.

(3) For different features have their own scattering characters, SAR, as a powerful tool for crop monitoring, can be used to map rice area effectively. Then considering the rice growing factors, rice yield can be estimated accurately.

Acknowledgements This work was supported by the National Natural Science Foundation of China (Grant No. 40171070) and the Knowledge Innovation Project of the Chinese Academy of Sciences (Grant No. CX010014). We would like to thank European Space Agency for providing ENVISAT ASAR data, and the Chinese Academy of Sciences and the Chinese Academy of Forestry for field data collection and data analysis.

References

1 Holecz F, Dwyer E, Monaco S, et al. An operational rice field mapping tool using spaceborne SAR data. ERS-ENVISAT Symposium, Göteborg, October. 2000
2 Thuy L T, Florence R, Wang L F, et al. Rice crop mapping and monitoring using ERS-1 data based on experiment and modeling results. IEEE Trans Geosci Remote Sensing, 1997, 35(1): 41－56
3 Brakke T W, Kanemasu E T, Steiner J L, et al. Microwave radar response to canopy moisture, Leaf-Area Indx, and dry weight of wheat, corn and sorghum. Remote Sensing Environ, 1981, 11: 207－220
4 Cloutis E A, Connery D R, Dover F J. Agricultural crop monitoring using airborne multi-spectral imagery and C-band synthetic aperture radar. Int J Remote Sensing, 1999, 20(4): 767－787
5 Mcnairn H, Ellis J, Van Der Sanden J J, et al. Providing crop information using RADARSAT-1 and satellite optical imagery. Int J Remote Sensing, 2002, 23(5): 851－870
6 Takashi K, Masaharu F, Kazuo C. Monitoring of rice crop growth from space using the ERS-1 C-band SAR. IEEE Trans Geosci Remote Sensing, 1995, 33(4): 1093－1096
7 Thuy L T, Henri L, Eric M, et al. Multitemporal and dural-polarization observations of agricultural aegetation aovers by X-band SAR Images. IEEE Trans Geosci Remote Sensing, 1989, 27(6): 709－718
8 Shao Y, Fan X T, Liu H, et al. Rice monitoring and production estimation using multitemporal RADARSAT. Remote Sensing Environ, 2001, 76: 310－325
9 Shao Y, Liao J J, Wang C Z. Analysis of temporal radar backscatter of rice: a comparison of SAR observations with modelling results. Can J Remote Sensing, 2002, 28(2): 128－138
10 Inoue Y, Kurosu T, Maeno H, et al. Season-long daily measurements of multifrequency (Ka, Ku, X, C, and L) and full-polarization backscatter signatures over paddy rice field and their relationship with biological variables. Remote Sensing En-

viron, 2002, 81: 194－204

11 Zeng Q M, Ma H B, Zhang T. Study and computing of rice backscattering coefficients. Acta Sci Nat Univ Pek (in Chinese), 2000, 36(1): 131－141

12 Sun G Q, Simonett D S. A composite L-band radar backscattering model for coniferous forest stands. Photogram Eng Remote Sensing, 1988, 54(8): 1195－1201

13 Fawwaz T U, Richard K M, Adrian K F. Microwave Remote Sensing-Active and Passive, Volume Ⅲ, Michigan: Aztech House, 1986. 1087－1088

14 Ulaby F T, Sarabandi K, Mcdonald K, et al. Michigan microwave canopy scattering model. Int J Remote Sensing, 1990, 11: 1223－1253

15 Karam M A, Fung A K, Lang R H, et al. A microwave scattering model for layered vegetation. IEEE Trans Geosci Remote Sensing, 1992, 30: 764－784

16 Bracaglia M, Ferrazzoli P, Guerriero L. A fully polarimetric multiple scattering for crops. Remote Sensing Environ, 1995, 54: 170－179

17 Fung A K, Microwave Scattering and Emission Models and Their Applications, London: Artech House, 1994

18 Sun G Q, David S S. Simulation of L-band HH microwave backscattering from coniferous forest stands: a comparison with SIR-B cata. Int J Remote Sensing, 1988, 9(5): 907－925

19 Fawwaz T U, Mohamed A. El-rayes. Microwave dielectric spectrum of vegetation-part Ⅱ: dual-dispersion model. IEEE Trans Geosci Remote Sensing, 1987, GE-25(5): 541－549